

Dynamical essence of the eccentric von Zeipel–Lidov–Kozai effect in restricted hierarchical planetary systems

Hanlun Lei¹ & Yan-Xiang Gong²

¹ School of Astronomy and Space Science and Key Laboratory of Modern Astronomy and Astrophysics in Ministry of Education, Nanjing University, Nanjing 210023, China
e-mail: leihl@nju.edu.cn

² College of Physics and Electronic Engineering, Taishan University, Taian 271000, China

Received; accepted

ABSTRACT

Aims. The eccentric von Zeipel–Lidov–Kozai (ZLK) effect is widely used to explain dynamical phenomena in varieties of astrophysical systems. The purpose of this work is to make clear the dynamical essence of the eccentric ZLK effect by constructing an inherent connection between such an effect and dynamics of secular resonance in restricted hierarchical planetary systems.

Methods. Dynamical structures of apsidal resonance are analytically studied by means of perturbative treatments. The resonant model is formulated by averaging the Hamiltonian (up to octupole order) over rotating ZLK cycles, producing an additional motion integral. The phase portraits under the resonant model can be used to analyse dynamical structures, including resonant centres, dynamical separatrices and islands of libration.

Results. By analysing phase portraits, five branches of libration centres and eight libration zones are found in the eccentricity–inclination space. There is an excellent agreement between analytical results of libration zone and numerical distributions of resonant orbit, indicating that the resonant model for apsidal resonances is valid and applicable. Additionally, it is found that, in the test-particle limit, distributions of flipping orbits are dominated by those apsidal resonances centred at the inclination of $i = 90^\circ$.

Conclusions. The eccentric ZLK effect is dynamically equivalent to the effect of apsidal resonance in restricted hierarchical planetary systems. The dynamical response of the eccentric ZLK effect (or effect of apsidal resonance) is to significantly excite eccentricities and/or inclinations of test particles in the very long-term evolution.

Key words. planets and satellites: dynamical evolution and stability – methods: analytical

1. Introduction

Hierarchical three-body configurations are common in varieties of astrophysical systems, ranging from the satellite and planet scales to supermassive black hole (Naoz 2016). Under the test-particle approximation, such a configuration reduces to the so-called restricted hierarchical three-body problem, where the test particle moves around the central body under the gravitational perturbation from the perturber. When the perturber moves on a circular orbit, Kozai (1962) and Lidov (1962) studied long-term dynamics of test particles and they found that a resonance occurs between the longitude of pericentre ϖ and the longitude of ascending node Ω when the inclination is greater than 39.2° . In the long-term evolution, coupled oscillations between eccentricity and inclination are called the standard Kozai–Lidov oscillations (or Kozai–Lidov effect) (Lithwick & Naoz 2011). About the same issue, Ito & Ohtsuka (2019) pointed out that von Zeipel (1910) performed a similar analysis; thus they suggested to refer to such a mechanism as the von Zeipel–Lidov–Kozai (ZLK) effect.

Under the circular assumption (for the orbit of perturber), the vertical angular momentum $H = \sqrt{1 - e^2} \cos i$ is conserved in the long-term evolution, showing that the orbits of test particle cannot flip between prograde and retrograde. It means that the standard ZLK effect cannot lead to the phenomenon of orbit flips. However, the situation is different when the circular as-

sumption is relaxed. In this context, the Hamiltonian needs to be formulated up to the octupole order in the semimajor axis ratio. Under the octupole-level approximation, the vertical angular momentum is no longer constant (Naoz 2016). In particular, long-timescale modulations of Kozai–Lidov cycle can force the variation of vertical angular momentum H , leading to striking features including flipping between prograde and retrograde, extremely high eccentricities and chaotic behaviours (Katz et al. 2011). Such a mechanism can be naturally referred to as the eccentric ZLK effect (Ito & Ohtsuka 2019), which have been used to interpret various dynamical phenomena in astrophysical systems (Libert & Tsiganis 2009; Shevchenko 2016; Naoz 2016). In the test-particle limit, Antognini (2015) investigated timescales of ZLK oscillations at quadrupole and octupole-order dynamical models.

Naoz et al. (2011) found that planets' orbits can flip between prograde and retrograde with respect to the invariant plane of system due to the eccentric ZLK effect and they proposed a possible clue for forming hot Jupiters on retrograde orbits by combining the eccentric ZLK effect with tidal friction at the late stage. To analytically understand the eccentric ZLK effect, Katz et al. (2011) performed an average for the secular equations of motion over the period of Kozai–Lidov cycle and found a new constant of motion. In particular, they derived an analytical criterion for orbit flips. At the same time, Lithwick & Naoz (2011) performed a numerical investigation about the eccentric ZLK ef-

fect and they numerically map out the initial conditions where flipping orbits occur for various values of ϵ (ϵ stands for the contribution of the octupole-order Hamiltonian). By using surfaces of section and Lyapunov exponents, Li et al. (2014a) studied the chaotic and quasi-periodic evolutions caused by the eccentric ZLK effect. For the same topic, Li et al. (2014b) classified flipping orbits into two types: the low-eccentricity, high-inclination (LeHi) case and high-eccentricity, low-inclination (HeLi) case. They pointed out that the first-type of flipping orbit is governed by the joint effect of the quadrupole-order and octupole-order resonances and the second type of flipping orbit is dominated by the octupole-order resonances (Li et al. 2014a,b). Recently, Sidorenko (2018) interpreted the eccentric ZLK effect working in the low-eccentricity, high-inclination space as a resonant phenomenon. In a recent work (Lei 2022), a systematical study is performed for the dynamics of orbit flips caused by eccentric ZLK effect through three approaches: Poincaré surfaces of section, dynamical system theory (periodic orbit and invariant manifold), and perturbative treatments. Through these studies, the dynamical essence of flipping orbits is very clear: flipping orbits are a kind of quasi-periodic (or resonant) trajectory around stable, polar, periodic orbits (Sidorenko 2018; Lei 2022).

However, the dynamical essence of the eccentric ZLK effect is not clear. We know that the eccentric ZLK effect is the dynamical response under the octupole-level Hamiltonian model. It means that there must be a certain correspondence between the secular dynamics and the eccentric ZLK effect. Based on this consideration, the purpose of this work is twofold. The first one is to analytically explore the dynamical structures of secular resonances (apsidal resonances) under the octupole-level approximation by means of perturbative treatments developed by Henrard & Lemaître (1986) and Henrard (1990). This theory was adopted by Sidorenko (2018) to study the same topic. The second one is to construct the dynamical connection between the eccentric ZLK effect and apsidal resonances at the octupole-level approximation in restricted hierarchical planetary systems. Our results show that (a) the webs of apsidal resonance constitute basic backbones imbedded in the phase space, governing the very long-term dynamics of particles, (b) in the test-particle limit, the eccentric ZLK oscillations are attributed to the effect of apsidal resonance, and (c) only those apsidal resonances with centres at $i = 90^\circ$ may cause orbit flips.

Through this study, the inherent connection between the eccentric ZLK effect and apsidal resonances becomes clear: from the viewpoint of dynamics, the eccentric ZLK effect is equivalent to the effect of apsidal resonance under the octupole-level approximation in restricted hierarchical planetary systems. The dynamical consequence of the eccentric ZLK effect (or effect of apsidal resonance) is to significantly excite eccentricities and/or inclinations of test particles in the long-term evolution. In particular, the behaviour of orbit flip is just one kind of dynamical response due to the eccentric ZLK effect (or effect of apsidal resonance). In this sense, the present work can be considered as an extension about the resonant interpretation for the eccentric ZLK effect (Sidorenko 2018).

The remaining part of this work is organised as follows. In Section 2, the Hamiltonian model is briefly introduced under the test-particle and octupole-order approximation. In Section 3, the fundamental frequencies and nominal location of apsidal resonance are identified under the quadrupole-order Hamiltonian flow. Resonant model for apsidal resonances is formulated in Section 4 by means of first-order perturbation theory. Results including the dynamical structures, libration zones and applica-

tions are presented in Section 5. Finally, conclusions of this work are summarised in Section 6.

2. Hamiltonian model

In this work, secular resonances are investigated for an inner test particle moving around a central star under the gravitational perturbation from a distant planet¹. Such a dynamical model is called restricted hierarchical planetary system, which is widely adopted as the basic dynamical model to study secular dynamics in varieties of astrophysical systems (Lithwick & Naoz 2011; Li et al. 2014a,b; Sidorenko 2018; Luo et al. 2016; Lei et al. 2018; Lei 2019; Katz et al. 2011; Antognini 2015; Lei 2021b,a, 2022). The mass of the central star is denoted by m_0 and the mass of the perturber is denoted by m_p . In the test-particle limit, the orbit of the perturber around the central star is unchanged, while the test particle moves around the central star on a perturbed Keplerian orbit. Under such a hierarchical configuration, the invariant plane of system is coincident with the orbit of perturber.

For convenience, let us introduce a right-handed inertial reference frame, with the origin at the central star, x - y plane at the invariable plane (i.e., the perturber's orbit), x -axis along the eccentricity vector of the perturber's orbit and z -axis parallel to the vector of the total angular momentum. Under such a coordinate system, the orbits of test particle (perturber) are described by the semimajor axis $a(a_p)$, the eccentricity $e(e_p)$, inclination $i(i_p)$, longitude of ascending node $\Omega(\Omega_p)$, argument of pericentre $\omega(\omega_p)$ and mean anomaly $M(M_p)$. For both prograde and retrograde configurations, the longitude of pericentre and mean anomaly can be defined in a general manner (Shevchenko 2016)

$$\varpi = \Omega + \text{sign}(\cos i)\omega, \quad \lambda = M + \varpi$$

for the test particle and

$$\varpi_p = \Omega_p + \text{sign}(\cos i_p)\omega_p, \quad \lambda_p = M_p + \varpi_p$$

for the perturber. Here $\text{sign}(x)$ is a sign function of x and it is equal to 1.0 when x is greater than zero and it is equal to -1.0 when x is smaller than zero. Under the chosen reference frame, it holds $i_p = 0$ and $\varpi_p = 0$ ². Without otherwise stated, in the entire work we adopt the variables with subscript p for the perturber and the ones without subscripts for test particle.

In the long-term evolution, the short-period terms arising in the Hamiltonian can be filtered out by means of double-averaging techniques over the orbital periods of the test particle and the perturber (Ford et al. 2000; Naoz et al. 2013; Naoz 2016; Luo et al. 2016; Shevchenko 2016; Lei et al. 2018; Lei 2019). Such a process of phase averaging is called secular approximation (Naoz 2016). Due to the hierarchical configuration, the semimajor axis ratio $\alpha = \frac{a}{a_p}$ is a small parameter, leading to the fact that the Hamiltonian can be truncated at a certain order in semimajor axis ratio³.

The (normalised) double-averaged Hamiltonian, up to the octupole order in the semimajor axis ratio, can be written as (Lithwick & Naoz 2011; Naoz 2016)

$$\mathcal{H} = -\left(F_{\text{quad}} + \epsilon F_{\text{oct}}\right) \quad (1)$$

¹ The planet acts the role of perturber.

² This is due to the setting that the x -axis is along the eccentricity vector of the perturber's orbit.

³ The Hamiltonian truncated at the second order corresponds to the quadrupole-level approximation, and the one truncated at the third order corresponds to the octupole-level approximation.

where the coefficient ϵ , measuring the significance of the octupole-order contribution, is a small parameter, given by

$$\epsilon = \frac{a}{a_p} \frac{e_p}{1 - e_p^2}$$

showing that the semimajor axis ratio $\alpha = \frac{a}{a_p}$ or the eccentricity of the perturber e_p is larger, the contribution of the octupole-order term is greater. The quadrupole-order term is given by

$$F_{\text{quad}} = -\frac{1}{2}e^2 + \cos^2 i + \frac{3}{2}e^2 \cos^2 i + \frac{5}{2}e^2 (1 - \cos^2 i) \cos(2\omega)$$

and the octupole-order term is given by

$$\begin{aligned} F_{\text{oct}} = & \frac{5}{16} \left(e + \frac{3}{4}e^3 \right) \\ & \times \left[(1 - 11 \cos i - 5 \cos^2 i + 15 \cos^3 i) \cos(\omega - \Omega) \right. \\ & + (1 + 11 \cos i - 5 \cos^2 i - 15 \cos^3 i) \cos(\omega + \Omega) \left. \right] \\ & - \frac{175}{64} e^3 \left[(1 - \cos i - \cos^2 i + \cos^3 i) \cos(3\omega - \Omega) \right. \\ & + (1 + \cos i - \cos^2 i - \cos^3 i) \cos(3\omega + \Omega) \left. \right] \end{aligned}$$

The double-averaged Hamiltonian up to an arbitrary order in α can be found in [Laskar & Boué \(2010\)](#) and [Lei \(2021a\)](#).

In order to formulate the Hamiltonian model, a set of (normalised) Delaunay variables are introduced as follows ([Lithwick & Naoz 2011](#)):

$$\begin{aligned} g = \omega, \quad G = \sqrt{1 - e^2}, \\ h = \Omega, \quad H = G \cos i. \end{aligned}$$

In terms of Delaunay's variables, the Hamiltonian can be further expressed as follows:

$$\begin{aligned} \mathcal{H}(g, h, G, H) = & \mathcal{H}_2(g, G, H) + \mathcal{H}_3(g, h, G, H) \\ = & -F_{\text{quad}}(g, G, H) - \epsilon F_{\text{oct}}(g, h, G, H), \end{aligned} \quad (2)$$

which determines a dynamical model with two degrees of freedom. Hamiltonian canonical relations lead to the equations of motion as follows ([Morbidelli 2002](#)):

$$\begin{aligned} \frac{dg}{dt} = \frac{\partial \mathcal{H}}{\partial G}, \quad \frac{dG}{dt} = -\frac{\partial \mathcal{H}}{\partial g}, \\ \frac{dh}{dt} = \frac{\partial \mathcal{H}}{\partial H}, \quad \frac{dH}{dt} = -\frac{\partial \mathcal{H}}{\partial h}. \end{aligned} \quad (3)$$

The Hamiltonian given by Eq. (2) holds the following symmetries ([Sidorenko 2018](#)):

$$\mathcal{H}(g, h, G, H) = \mathcal{H}(2\pi - g, h, G, -H) = \mathcal{H}(g, 2\pi - h, G, -H),$$

which implies that the solution curves under the Hamiltonian flow are symmetric with respect to $H = 0$ (i.e., $i = 90^\circ$). It is noted that there is a unique parameter (ϵ) that characterizes the dynamical model. The effectiveness of the standard double-averaging process requires that ϵ should be a small parameter ($\epsilon \ll 1$) and the mass of the perturber should be much smaller than that of the central star ($m_p \ll m_0$) ([Naoz 2016](#); [Luo et al. 2016](#); [Lei et al. 2018](#); [Lei 2019](#)). For all the following simulations, the dynamical model with system parameter $\epsilon = 0.03$ is adopted as an example⁴.

⁴ Without doubt, the method adopted in this work is applicable to dynamical models specified by other values of ϵ .

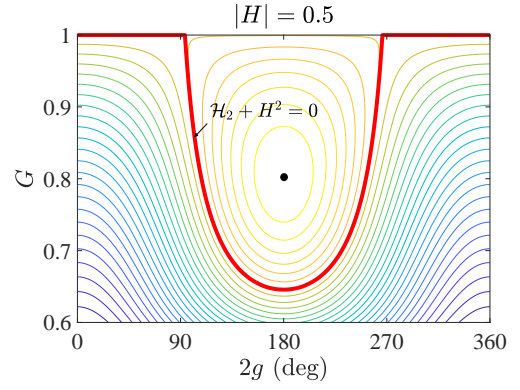


Fig. 1. Phase portrait (level curves of Hamiltonian in the phase space) with the motion integral at $|H| = 0.5$ (corresponding to the critical inclination at $i_c = 60^\circ$ or $i_c = 120^\circ$) under the quadrupole-order Hamiltonian model. Kozai centre is marked by black dot and dynamical separatrix is shown in red line. The regions filled with circulating and librating ZKL cycles are divided by the dynamical separatrix expressed by $\mathcal{H}_2 + H^2 = 0$. For the current example, the phase space with $\mathcal{H}_2 > -0.25$ is of ZKL libration and the space with $\mathcal{H}_2 < -0.25$ is of ZKL circulation.

3. Nominal location of apsidal resonance

In this section, let us identify the fundamental frequencies under the quadrupole-order dynamical model and then it becomes possible for us to determine the nominal location of secular resonance.

The quadrupole-order Hamiltonian \mathcal{H}_2 is very simple and can be written as

$$\begin{aligned} \mathcal{H}_2 = & \frac{1}{2} (1 - G^2) - \frac{H^2}{G^2} - \frac{3}{2} \left(\frac{1}{G^2} - 1 \right) H^2 \\ & - \frac{5}{2} \left(1 - G^2 + H^2 - \frac{H^2}{G^2} \right) \cos(2g) \end{aligned} \quad (4)$$

where the angular coordinate h is absent from \mathcal{H}_2 , indicating that the z -component of the angular momentum H is conserved under the quadrupole-order model. The conserved quantity H can be specified by the critical inclination i_c (when the eccentricity is assumed as zero) of the manner ([Kozai 1962](#)),

$$H = \sqrt{1 - e^2} \cos i = \cos i_c.$$

In the following discussions, we often use i_c to stand for H . The dynamical model determined by \mathcal{H}_2 is of one degree of freedom. With given H (or i_c), the solution curves under the Hamiltonian flow of \mathcal{H}_2 are usually called the ZKL cycles, including librating ZKL cycles and rotating ZKL cycles. Rotating and librating ZKL cycles are divided by means of a dynamical separatrix in the phase space.

The global structures in the phase space can be explored by analysing phase portraits, which correspond to level curves of Hamiltonian with given motion integral. As an example, the case of $|H| = 0.5$ (corresponding to the critical inclination at $i_c = 60^\circ$ or $i_c = 120^\circ$) is considered and the associated phase portrait is presented in Fig. 1. In this case, the Kozai–Lidov resonance may occur. At the ZKL centre, the eccentricity and inclination should satisfy ([Kozai 1962](#))

$$\cos^2 i = \frac{3}{5} (1 - e^2).$$

In Fig. 1, the black dot stands for the position of ZKL centre, at which the Hamiltonian takes its maximum. The dynamical separatrix, as shown in red line, divides the rotating ZKL cycles from librating ZLK cycles. It is known that the separatrix corresponds to the level curve of Hamiltonian passing through $G = 1$ (corresponding to $e = 0$). Substituting $G = 1$ into the quadrupole-order Hamiltonian \mathcal{H}_2 given by Eq. (4), it is not difficult to get the expression of separatrix as (Lei 2021b)

$$\mathcal{H}_2 + H^2 = 0.$$

For the current example (the motion integral is taken as $|H| = 0.5$), the Hamiltonian of separatrix is equal to $\mathcal{H}_2 = -0.25$. From the phase portrait, we observe that, in the phase space, the region with $\mathcal{H}_2 > -0.25$ is of ZLK libration and the region with $\mathcal{H}_2 < -0.25$ is of ZLK circulation.

From Fig. 1, we can further observe that the ZLK cycles starting from $2g = 0$ are of circulation. In the following, we will focus on those regions filled with rotating ZLK cycles⁵ where the octupole-order resonances may appear and dominate the long-term dynamics. Without loss of generality, we fix the initial condition at $2g = 0$ for rotating ZLK cycles (Katz et al. 2011; Li et al. 2014a; Sidorenko 2018; Lithwick & Naoz 2011) and then determine the fundamental frequencies in the parameter space spanned by orbit elements (e, i) or conserved quantities (\mathcal{H}_2, H).

In order to study the dynamics of secular resonance by means of perturbative treatments (Henrard & Lemaître 1986; Henrard 1990), let us introduce the following action–angle variables under the quadrupole-order Hamiltonian flow,

$$\begin{aligned} g^* &= g - \rho_g(g^*, G^*, H^*), & G^* &= \frac{1}{2\pi} \int_0^{2\pi} G dg, \\ h^* &= h - \rho_h(g^*, G^*, H^*), & H^* &= H, \end{aligned} \quad (5)$$

which is canonical with the generating function,

$$S_1(g, h, G^*, H^*) = hH^* + \int G(\mathcal{H}_2(G^*, H^*), g, H^*) dg.$$

In Eq. (5), ρ_g and ρ_h are periodic functions with the same period of the rotating ZLK cycle. The variable G^* is called Arnold action, which stands for the phase-space area bounded by the ZLK cycle (divided by 2π).

Under the quadrupole-order dynamical model, let us denote the period of g as T_g and the period of h as T_h . Thus, the linear functions of g^* and h^* can be expressed as

$$g^* = \frac{2\pi}{T_g} t, \quad h^* = h_0^* + \frac{2\pi}{T_h} t.$$

At the initial instant, it holds $g^* = 0$ and $h^* = h_0^*$ for rotating ZLK cycles.

In Fig. 2, a rotating ZLK cycle in the phase space (g, G) is shown in the left panel and the relation between the Arnold action G^* and $G(0)$ is plotted in the right panel. In the left panel, the location of G^* for the particular example is marked in red. Evidently, G^* is a constant under the quadrupole-order Hamiltonian flow.

⁵ It is noted that, inside the regions filled with ZLK librating cycles, the dynamics is dominated by the quadrupole-order resonance (i.e., ZLK resonance). Only in those regions filled with ZLK rotating cycles, the octupole-order resonance plays an important role in governing the very long-term behaviours of particles (Li et al. 2014a).

In practice, we produce the ZLK cycle as well as the action G^* by integrating the following differential equations over one period of ZLK cycle (i.e., T_g) under the quadrupole-order Hamiltonian flow,

$$\dot{g} = \frac{\partial \mathcal{H}_2}{\partial G}, \quad \dot{G} = -\frac{\partial \mathcal{H}_2}{\partial g}, \quad \dot{W} = G \frac{\partial \mathcal{H}_2}{\partial G}.$$

At the initial instant, it holds $g_0 = 0$ and $W_0 = 0$. Here $W(t)$ stands for the oriented area enclosed by the solution curve $G(g)$ under the quadrupole-level Hamiltonian flow. In particular, when the integration time is equal to one period of the rotating ZLK cycle, it holds

$$W(T_g) = \int_0^{T_g} G \frac{\partial \mathcal{H}_2}{\partial G} dt = \int_0^{2\pi} G dg = 2\pi G^*.$$

Thus, the Arnold action G^* is equal to $\frac{1}{2\pi} W(T_g)$. It is mentioned that the ZLK cycles $G(g)$ and the Arnold action G^* can be alternatively produced by means of elliptic integrals, as presented by Sidorenko (2018).

According to the generating function, we can obtain an alternative expression for the new set of angles (g^*, h^*) as follows:

$$g^* = \frac{\partial S_1}{\partial G^*}, \quad h^* = \frac{\partial S_1}{\partial H^*}.$$

Thus, we can get the expressions for computing periodic functions $\rho_g = g - g^*$ and $\rho_h = h - h^*$ as

$$\begin{aligned} \rho_g(g^*, G^*, H^*) &= \int \frac{\partial \mathcal{H}_2}{\partial G} dt \\ &\quad - \frac{\partial}{\partial G^*} \int G(\mathcal{H}_2(G^*, H^*), g, H^*) dg, \\ \rho_h(g^*, G^*, H^*) &= -\frac{\partial}{\partial H^*} \int G(\mathcal{H}_2(G^*, H^*), g, H^*) dg, \end{aligned}$$

which indicate that $\rho_g = g - g^*$ and $\rho_h = h - h^*$ are equal to zero when $g^* = 0$ or $g^* = 2\pi$ (Henrard 1990). It means that the old and new set of angles are coincident at the initial instant and at one period of ZLK cycle.

For the example shown in the left panel of Fig. 2, the time histories of (g, h) and (g^*, h^*) are shown in the left panel of Fig. 3 and the differences between the old and new set of angles ρ_g and ρ_h as functions of g^* are reported in the right panel of Fig. 3. It is observed that (a) the new angles g^* and h^* are linear functions of time, and (b) ρ_g and ρ_h are periodic functions of g^* and they are equal to zero when g^* is at $0, \pi/2, \pi, 3\pi/2$ and 2π .

Under the canonical transformation given by Eq. (5), the quadrupole-level Hamiltonian \mathcal{H}_2 becomes (Henrard 1990)

$$\mathcal{H}_2(g, G, H) = \mathcal{H}_2(G^*, H^*), \quad (6)$$

which shows that g^* and h^* are absent from the Hamiltonian \mathcal{H}_2 , indicating that G^* and H^* are conserved quantities along the ZLK cycle. The fundamental frequencies under the quadrupole-order dynamical model are identified by

$$\dot{g}^* = \frac{\partial \mathcal{H}_2(G^*, H^*)}{\partial G^*}, \quad \dot{h}^* = \frac{\partial \mathcal{H}_2(G^*, H^*)}{\partial H^*} \quad (7)$$

which determines the periods of g and h as

$$T_g = \frac{2\pi}{\dot{g}^*}, \quad T_h = \frac{2\pi}{\dot{h}^*}.$$

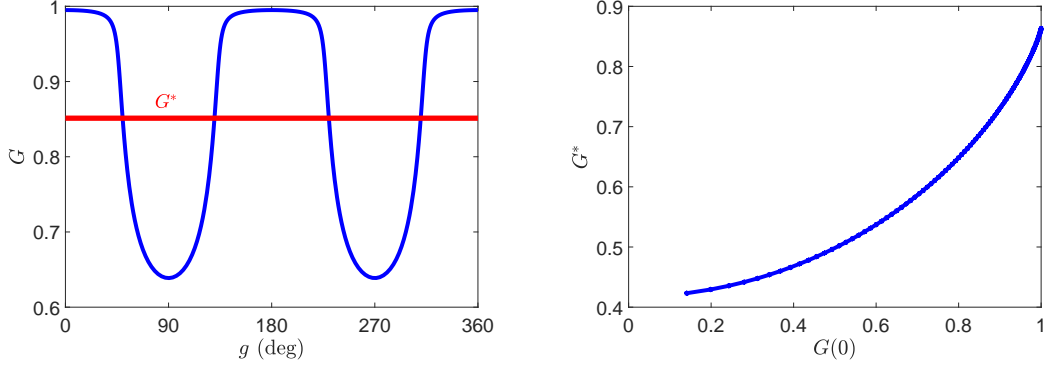


Fig. 2. An example of rotating ZLK cycle shown in the phase space (*left panel*) and the Arnold action G^* as a function of $G(0)$ (*right panel*), under the quadrupole-order Hamiltonian flow. Please refer to the text for the definition of the Arnold action G^* . For the example shown in the left panel, the initial condition is taken as $g_0 = 0$, $h_0 = 2\pi$, $G_0 = 0.9950$ and $H_0 = 0.4975$.

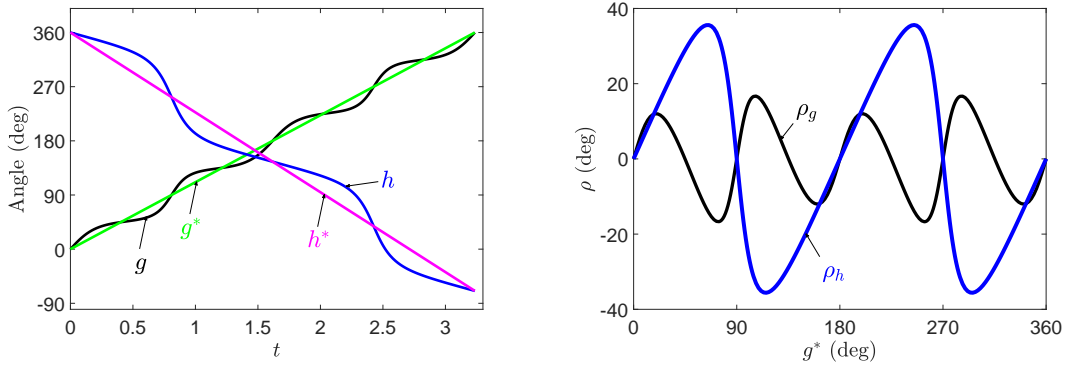


Fig. 3. Old and new sets of angular coordinates (g, h) and (g^*, h^*) as functions of time (*left panel*) as well as the differences between them $\rho_g = g - g^*$ and $\rho_h = h - h^*$ as functions of g^* (*right panel*). These two plots correspond to the example shown in the left panel of Fig. 2.

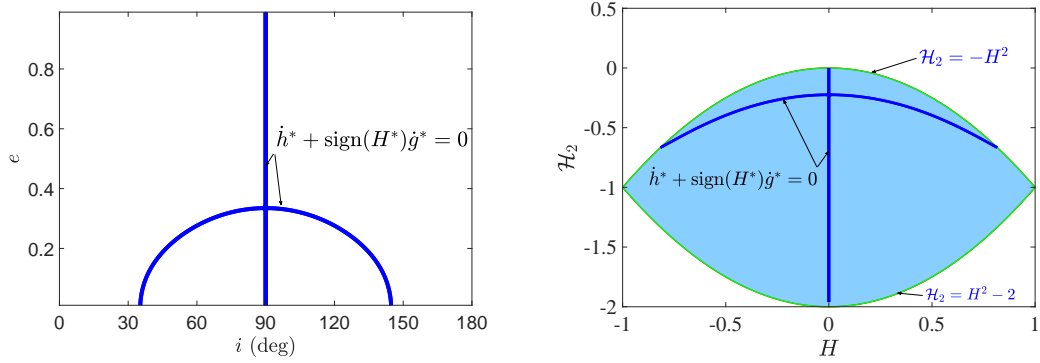


Fig. 4. Nominal location of apsidal resonance with critical argument of $\sigma_1 = h^* + \text{sign}(H^*)g^*$, shown in the (i, e) space (*left panel*) and in the (H, \mathcal{H}_2) space (*right panel*). The shaded region in the right panel is of ZLK circulation.

Based on the fundamental frequencies, it is possible for us to determine the nominal location of secular resonance by the following resonant condition,

$$k_1 \dot{g}^* + k_2 \dot{h}^* = 0, \quad (8)$$

where $k_1, k_2 \in \mathbb{Z}$.

As for the octupole-order resonance, the critical argument is given by

$$\sigma = h^* + \text{sign}(H^*)g^*.$$

In Fig. 4, the solution of $\dot{\sigma} = \dot{h}^* + \text{sign}(H^*)\dot{g}^* = 0$ ⁶ is distributed in the (i, e) space in the left panel and in the (H, \mathcal{H}_2) space in the right panel. In the left panel, the eccentricity and inclination are evaluated when the angle g is equal to zero⁷. In the right panel, the shaded region is of ZLK circulation, the upper boundary of circulation region is given by $\mathcal{H}_2 + H^2 = 0$ and the bottom boundary is given by $\mathcal{H}_2 - H^2 + 2 = 0$ (Lei 2021b). In both panels, the

⁶ It corresponds to $k_1 = 1$ and $k_2 = \text{sign}(H^*)$, means that k_2 is related to the inclination.

⁷ This is because we fix $2g = 0$ as initial conditions of rotating ZLK cycles.

distribution of nominal location of resonant centre is symmetric with respect to $i = 90^\circ$ (or $H = 0$).

From the left panel of Fig. 4, we can observe that there are three branches of resonant centres in the considered parameter space: one branch corresponds to polar orbits at arbitrary eccentricities and the other two branches occupy the low-eccentricity space. The latter two branches are called asymmetric families of resonant centre. From the right panel of 4, we can see that these two asymmetric branches are close to the upper boundary of circulation region represented by $\mathcal{H}_2 + H^2 = 0$ (this boundary corresponds to the ZLK separatrix, as discussed in Fig. 1).

Next, let us discuss the essence of the resonance with critical argument of $\sigma = h^* + \text{sign}(H^*)g^*$. According to the ‘general’ definition of longitude of pericentre ϖ^* for prograde and retrograde orbit configurations (Shevchenko 2016),

$$\varpi^* = \Omega^* + \text{sign}(\cos i^*)\omega^*,$$

we can see that the critical argument σ is equal to the longitude of pericentre ϖ^* . Because of the choice of the reference frame, it is known that the longitude of pericentre of the perturber’s orbit is fixed at zero, i.e., $\varpi_p = 0$ and $\dot{\varpi}_p = 0$. As a result, we can further write the critical argument as

$$\sigma = h^* + \text{sign}(H^*)g^* = \varpi^* = \varpi^* - \varpi_p \quad (9)$$

which means that, in essence, the resonances arising in Fig. 4 are the so-called apsidal resonances with critical argument of $\sigma = \varpi^* - \varpi_p$. For simplicity, we denote the critical argument of apsidal resonance as $\sigma = h^* + \text{sign}(H^*)g^*$ in the test-particle limit⁸. Based on the set of Delaunay variables (g, h, G, H) , Sidorenko (2018) defined the critical argument as $\sigma = h + \text{sign}(H)g$, which is also adopted by Lei (2022) in his study. Additionally, Katz et al. (2011) introduced the longitude $\Omega_e = \Omega + \arctan(\tan \omega \cos i)$ to describe the very long-term behaviours caused by eccentric ZLK effect. Discussions about the relation between Ω_e and $\sigma = h + \text{sign}(H)g$ are made in Lei (2022).

In the coming section, we will study the dynamics of apsidal resonance from the viewpoint of perturbative treatments developed by Henrard & Lemaître (1986) and Henrard (1990). The core concept is to consider the octupole-order term in the Hamiltonian as the perturbation to the quadrupole-order dynamics.

4. Resonant Hamiltonian of apsidal resonance

In the previous section, we know that the apsidal resonances with critical argument of $\sigma = h^* + \text{sign}(H^*)g^*$ can happen in the considered parameter space. The purpose of this section is to formulate the resonant Hamiltonian by means of first-order perturbation theory (Henrard 1990). This theory was also adopted by Sidorenko (2018).

Under the new set of canonical variables (g^*, h^*, G^*, H^*) , the Hamiltonian up to the octupole order in α can be expressed as

$$\mathcal{H}(g^*, h^*, G^*, H^*) = \mathcal{H}_2(G^*, H^*) + \mathcal{H}_3(g^*, h^*, G^*, H^*), \quad (10)$$

where the quadrupole-order Hamiltonian \mathcal{H}_2 (independent on the angular coordinates) is considered as the unperturbed part and the octupole-order Hamiltonian \mathcal{H}_3 plays the role of perturbation to the quadrupole-order dynamics⁹. In such a perturbed Hamiltonian model, the unperturbed part \mathcal{H}_2 is also called the

⁸ In the test-particle limit, the longitude of the perturber with $\varpi_p = 0$ is taken into account.

⁹ The magnitude of perturbation is measured by the small parameter ϵ .

kernel function, which yields the fundamental (or proper) frequencies.

In order to study the dynamics of apsidal resonance with critical argument of $\sigma = h^* + \text{sign}(H^*)g^*$, the following transformation is introduced,

$$\begin{aligned} \sigma_1 &= h^* + \text{sign}(H^*)g^*, & \Sigma_1 &= H^* \\ \sigma_2 &= g^*, & \Sigma_2 &= G^* - |H^*| \end{aligned} \quad (11)$$

which is canonical with the generating function,

$$S_2(g^*, h^*, \Sigma_1, \Sigma_2) = h^*\Sigma_1 + g^*(|\Sigma_1| + \Sigma_2).$$

It is noted that a similar transformation to Eq. (11) is introduced by Sidorenko (2018) and Lei (2022) but based on the set of canonical variables (g, h, G, H) .

Under the new set of canonical variables $(\sigma_1, \sigma_2, \Sigma_1, \Sigma_2)$, the Hamiltonian can be further written as

$$\mathcal{H}(\sigma_1, \sigma_2, \Sigma_1, \Sigma_2) = \mathcal{H}_2(\Sigma_1, \Sigma_2) + \mathcal{H}_3(\sigma_1, \sigma_2, \Sigma_1, \Sigma_2). \quad (12)$$

It should be mentioned that it is difficult to obtain the explicit expression of Eq. (12). In practice, we compute the Hamiltonian \mathcal{H} numerically once the set of variables $(\sigma_1, \sigma_2, \Sigma_1, \Sigma_2)$ is given.

At the resonant centre shown in Fig. 4, it holds

$$\dot{\sigma}_1 = \frac{\partial \mathcal{H}_2}{\partial \Sigma_1} = 0.$$

As the octupole-order Hamiltonian \mathcal{H}_3 is small compared to the quadrupole-order Hamiltonian \mathcal{H}_2 , we can obtain

$$\dot{\sigma}_1 = \frac{\partial \mathcal{H}}{\partial \Sigma_1} = \frac{\partial \mathcal{H}_2}{\partial \Sigma_1} + \frac{\partial \mathcal{H}_3}{\partial \Sigma_1} = \frac{\partial \mathcal{H}_3}{\partial \Sigma_1} \sim O(\epsilon)$$

which shows that, under the perturbation of the octupole-order interaction, apsidal resonances may also take place.

When the test particle is inside an apsidal resonance, the resonant angle σ_1 becomes a long-period variable and the angle σ_2 is a short-period variable. This is a separable Hamiltonian system (Henrard 1990). Thus, the terms involving σ_2 in the Hamiltonian yield short-period influences, thus they can be filtered out by means of averaging technique¹⁰. To this end, we can formulate the resonant Hamiltonian by performing a further average for the Hamiltonian over one period of σ_2 ,

$$\mathcal{H}^*(\sigma_1, \Sigma_1, \Sigma_2) = \frac{1}{2\pi} \int_0^{2\pi} \mathcal{H}(\sigma_1, \sigma_2, \Sigma_1, \Sigma_2) d\sigma_2. \quad (13)$$

Because of the definition $\sigma_2 = g^*$, we can understand that such an average is performed over one period of a rotating ZLK cycle under the quadrupole-order Hamiltonian flow (Sidorenko 2018; Katz et al. 2011). Under the dynamical model determined by Eq. (13), the angle σ_2 becomes a cyclic coordinate, so that its action Σ_2 becomes a constant of motion (or motion integral). The resulting resonant model determined by Eq. (13) is of one degree of freedom, depending on the motion integral Σ_2 .

When the eccentricity is assumed as zero, the motion integral Σ_2 can be specified by a critical inclination i_* ,

$$\Sigma_2 = G^* - |H^*| = 1 - |\cos i_*| \quad (14)$$

The critical inclination i_* corresponds to the minimum inclination in the prograde space and corresponds to the maximum inclination in the retrograde space. It is not difficult to get that i_* and $\pi - i_*$ stand for the same motion integral.

¹⁰ Averaging treatment corresponds to the lowest-order perturbation method (Naoz 2016).

5. Results

In the previous section, the resonant Hamiltonian for apsidal resonances is formulated as $\mathcal{H}^*(\sigma_1, \Sigma_1, \Sigma_2)$ where Σ_2 is the motion integral of the resonant model. The global dynamics of apsidal resonance in the phase space can be revealed by phase portraits. In this section, we produce phase portraits and then analyse the phase portraits to estimate resonant width (Lei 2021a; Lei & Li 2021; Lei 2022). At last, we construct a connection between the libration zones of apsidal resonance and numerical distributions of resonant orbit (or flipping orbit).

5.1. Dynamical structures of apsidal resonance

In Fig. 5, the (pseudo-) phase portraits are shown in the (σ_1, i_0) space for the motion integral specified by the critical inclination at $i_* = 30^\circ(150^\circ)$, $45^\circ(135^\circ)$, $50^\circ(130^\circ)$ and $65^\circ(115^\circ)$. It should be noted that i_0 given in the y -axis corresponds to the inclination when the angle g is equal to zero¹¹. Dynamical separatrices are marked in red lines and the resonant width, measuring the maximum size of the island of libration, is denoted by Δi_0 . Evidently, all the dynamical structures are symmetric with respect to the lines of $i_0 = 90^\circ$, due to the symmetry of the Hamiltonian function.

When the critical inclination is at $i_* = 30^\circ(150^\circ)$ (see the top-left panel of Fig. 5), the structure arising in the phase portrait is pendulum-like: there is one resonant centre and one saddle point. The resonant centre is located at $(\sigma_1 = 180^\circ, i_0 = 90^\circ)$ and the saddle point is located at $(\sigma_1 = 0^\circ, i_0 = 90^\circ)$. The single island of libration is bounded by the dynamical separatrix shown by red line. As for this low-inclination case, there is another island of libration arising in low-eccentricity space, which will be shown in Fig. 6.

When the critical inclination is increased up to $i_* = 45^\circ(135^\circ)$ (see the top-right panel of Fig. 5), the dynamical structures become complex. In total, there are three islands of libration: one is centred at $(\sigma_1 = 0, i_0 = 90^\circ)$ and the other two islands are centred at $(\sigma_1 = 180^\circ, i_0 \neq 90^\circ)$; the latter two islands of libration are symmetric with respect to $i_0 = 90^\circ$. There are three separatrices (shown by red lines), stemming from three saddle points. These separatrices provide boundaries for three isolated islands of libration in the phase space.

When the critical inclination is up to $i_* = 50^\circ(130^\circ)$ (see the bottom-left panel of Fig. 5), there are also three resonant centres and three saddle points. However, it is different from the case of $i_* = 45^\circ(135^\circ)$ because there are only two separatrices: an inner separatrix and an outer separatrix. The inner separatrix bounds two asymmetric islands of libration, and the outer separatrix bounds the island centred at $(\sigma_1 = 0, i_0 = 90^\circ)$ and the island centred at $(\sigma_1 = 180^\circ, i_0 = 90^\circ)$. The region bounded by the inner and outer separatrices is also of libration. The resonant trajectory inside this region holds the maximum variation of inclination up to $\sim 80^\circ$.

When the critical inclination is at $i_* = 65^\circ(115^\circ)$ (see the bottom-right panel of Fig. 5), the dynamical structure becomes pendulum-like again: there is a single island of libration, centred at $(\sigma_1 = 180^\circ, i_0 = 90^\circ)$. Along the resonant trajectory inside this island, the maximum variation of inclination can reach $\sim 50^\circ$.

The phase portraits shown by Fig. 5 indicate that the inclinations of test particles can be effectively excited following along the trajectories inside islands of libration. Such a significant vari-

ation of orbit orientation is due to the effect of apsidal resonance under the octupole-order Hamiltonian model.

For the low-inclination cases, two examples are presented in Fig. 6 for the cases of $i_* = 20^\circ(160^\circ)$ and $i_* = 30^\circ(150^\circ)$. Different from Fig. 5, the phase portraits are plotted in the (σ_1, e_0) space. Here e_0 corresponds to the eccentricity when the angle g is equal to zero. Besides the islands shown in Fig. 5 (see the top-left panel), a new island arises in the low-eccentricity space and is centred at $\sigma_1 = 0$. Also, the dynamical separatrices are shown in red lines. In these two plots, the resonant width is measured by Δe_0 . Following along the trajectories inside islands of libration, the eccentricities of test particles can be excited due to the effect of apsidal resonance.

5.2. Libration zones of apsidal resonance

By analysing phase portraits at different levels of motion integral Σ_2 , it is possible for us to identify the location of resonant centre and boundaries of libration zones.

The main results of this work are reported in Fig. 7, where the resonant centres are marked in black dots and libration zones are shown in shaded areas with different colors. Boundaries of each libration zone are provided by the dynamical separatrix evaluated at the angle of the corresponding resonant centre (see Figs. 5 and 6 for representative phase portraits). The level curves of the motion integral Σ_2 are plotted in dashed lines as background. It is noted that resonant width is measured along isolines of motion integral.

From Fig. 7, we can see that dynamical structures arising in the (e, i) space are symmetric with respect to the line of $i = 90^\circ$. In total, there are five branches of libration centres: one branch located on the polar line, two branches occupying in the low-eccentricity and low-inclination space and the remaining two located in the space with eccentricities changing from ~ 0 to ~ 0.4 . In addition, there are eight libration zones, denoted by numbers from 1 to 8. It should be noted that the branches of resonant centres in zones 1 and 2 are not present under the quadrupole-level dynamical model¹². It means that these two branches are present due to the pure effect of octupole-order Hamiltonian. Except for the zones 1 and 2, all the other branches of libration centres are consistent with the ones shown in Fig. 4.

As for libration zone 1 (see Fig. 6 for the representative phase portraits), the bottom boundary is located at $e = 0$ ¹³, the resonant width decreases first and then increases with the inclination i . Inside this zone, Funk et al. (2011) found an interesting dynamical region around $i \sim 35^\circ$, where the low-eccentricity orbits are long-term stable, meaning that the inclined ($\sim 35^\circ$) quasi-circular Earth-mass companion can be survived in the habitable zone of extrasolar system. Libert & Delsate (2012) explained that the long-term stable dynamics at inclination of $\sim 35^\circ$ is due to the existence of the secular resonance associated with $\sigma = \omega - \Omega$. In the low-eccentricity space with $i < 39^\circ$, Lei (2021a) studied the long-term dynamics by means of Lie series transformation and they pointed out the long-term stability inside this zone is governed by the apsidal resonance with argument of $\sigma = \omega + \Omega$, which is consistent with the result of the current work.

Libration zone 1 has a symmetric zone in the retrograde space, denoted by 2. As for this zone, the bottom boundary of libration is located at $e = 0$ and the resonant width decreases first and then increases with $\pi - i$. Inside zones 1 and 2, the effect of

¹² See Fig. 4 for the nominal location of apsidal resonance.

¹³ It shows that zero-eccentricity points $e = 0$ are saddle points of the associated resonant model.

¹¹ This is because we assume $2g = 0$ as the initial conditions for rotating ZLK cycles. This assumption is often used in this work.

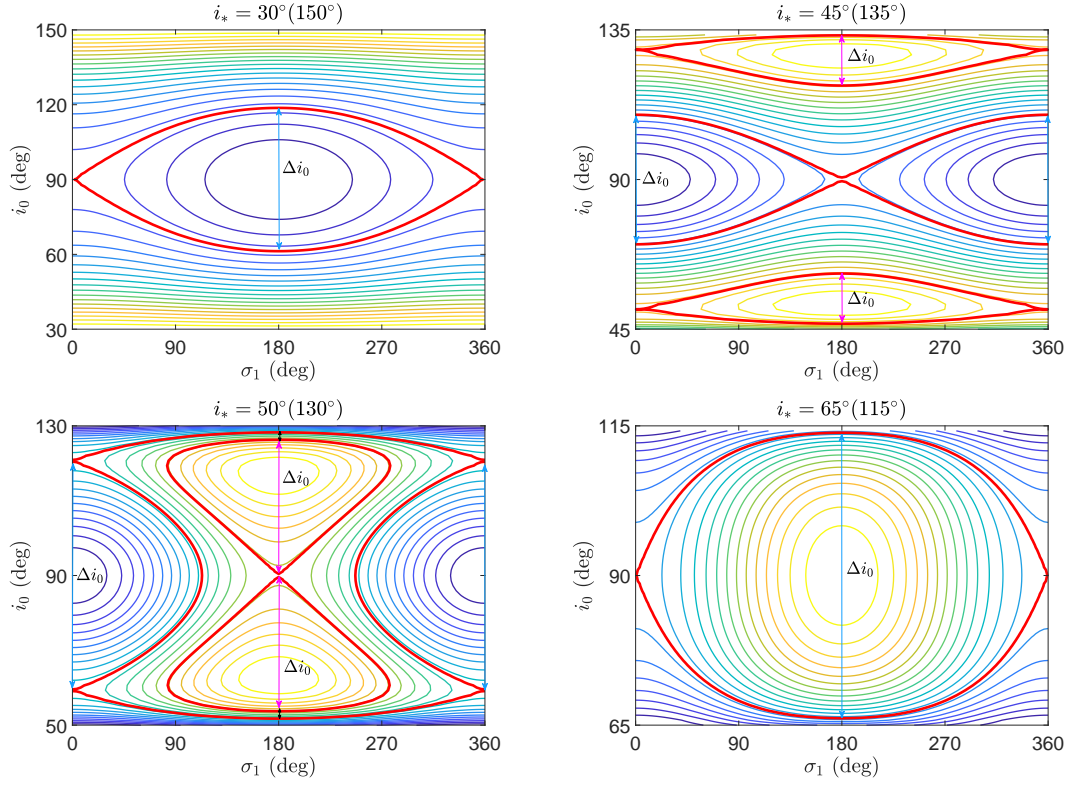


Fig. 5. Phase portraits (level curves of resonant Hamiltonian) of apsidal resonance with critical argument of $\sigma_1 = h^* + \text{sign}(H^*)g^*$ at different levels of motion integral specified by i_* . Here i_* represents the magnitude of motion integral Σ_2 (please refer to the text for details). It is noted that i_0 shown in the y-axis corresponds to the inclination when the angle g is equal to zero. Dynamical separatrices are marked in red lines. The resonant width, denoted by Δi_0 , measures the maximum size of island of libration.

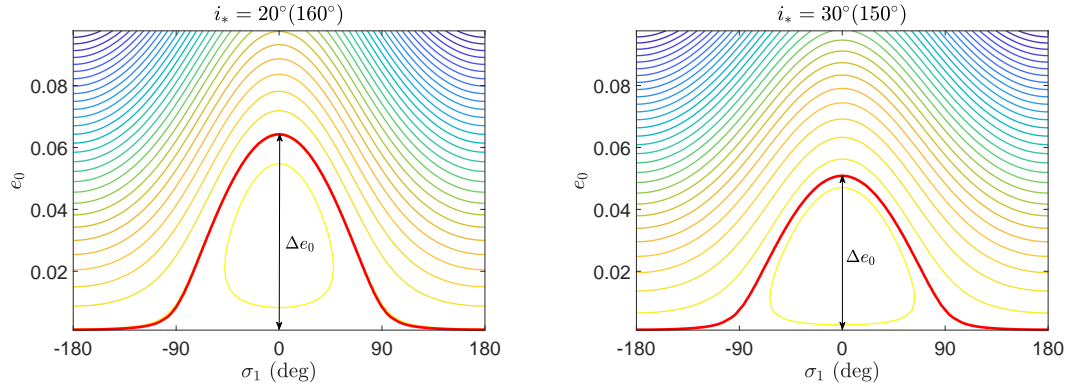


Fig. 6. Phase portraits (level curves of resonant Hamiltonian) for low-inclination cases, shown in the (σ_1, e_0) space. Note that e_0 is the eccentricity when the angle g is equal to zero. Dynamical separatrices are marked in red lines. The resonant width, denoted by Δe_0 , measures the maximum size of island of libration.

apsidal resonance is to excite the eccentricities. However, the inclination has little variation during the long-term evolution. This is the reason that the low-eccentricity islands of libration cannot be found in the phase portrait plotted in the (σ_1, i_0) space (please refer to the first panel of Fig. 5).

Libration zone 3 appears when the critical inclination is larger than $\sim 59^\circ$ and smaller than $\sim 121^\circ$ (see the bottom-right panel of Fig. 5 for the representative phase portrait). The eccentricity of this zone ranges from zero to ~ 0.35 . The effect of apsidal resonance inside this zone is to exchange the test particle's eccentricity and inclination. The resonant trajectories inside this zone hold resonant centres at $i = 90^\circ$. Thus all the trajectories

inside this zone could flip from prograde to retrograde and back again.

There are two subregions in zone 4: one in the prograde space and the other one in the retrograde space. According to the phase portrait shown in the bottom-left panel of Fig. 5, we can see that this zone of libration holds centres at $i = 90^\circ$ and it is bounded by the inner and outer separatrices. The effect of apsidal resonance inside this zone is to significantly change test particle's eccentricity and inclination. In addition, all the trajectories inside this zone could realise flips between prograde and retrograde.

Zones 5 and 6 are symmetric with respect to $i = 90^\circ$. Please refer to the top-right panel of Fig. 5 for the representative phase

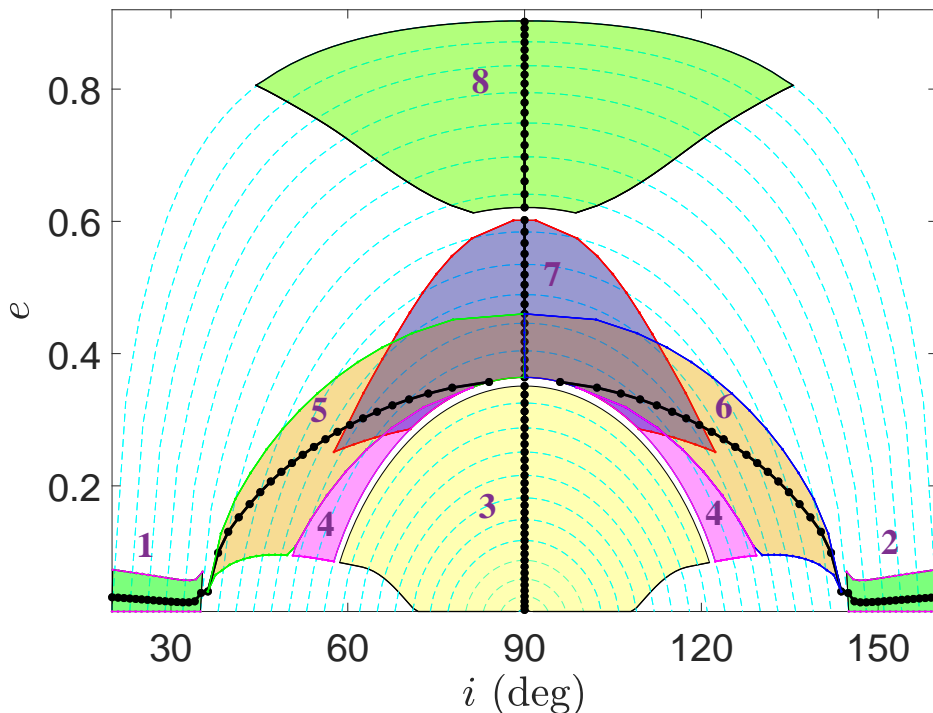


Fig. 7. Resonant centres of apsidal resonance distributed in the inclination–eccentricity space (black dots) and libration zones obtained by analysing phase portraits (shaded areas). The level curves of the motion integral Σ_2 are shown as background and the resonant width is measured along the isoline of Σ_2 . Totally, there are eight libration zones, denoted by numbers from 1 to 8. Evidently, the distribution of libration zones is symmetric with respect to the line of $i = 90^\circ$.

portrait. We can see that, for these two zones, the line of $i = 90^\circ$ provides one boundary, so that the resonant trajectories are restrained in either the prograde space or the retrograde space. It means that the trajectories inside these two zones cannot flip from prograde to retrograde or vice versa.

Let us move to the last two zones 7 and 8. Please refer to the top-left and -right panels of Fig. 5 for representative phase portraits. Zone 7 is located in the intermediate-eccentricity region, and zone 8 is located in the high-eccentricity region. Both of them hold resonant centres at $i = 90^\circ$. As a result, all the resonant trajectories inside these two zones can flip from prograde to retrograde and back again.

Figures 8 and 9 provide comparisons between analytical and numerical results for the libration zones of apsidal resonance. In particular, Fig. 8 corresponds to apsidal resonances centred at $\sigma_{1,c} = \pi$ and Fig. 9 corresponds to the ones centred at $\sigma_{1,c} = 0$. For analytical results, libration zones 3, 4, 5, 6 and 8 are shown in the left panel of Fig. 8 and libration zones 1, 2 and 7 are presented in the left panel of Fig. 9. To be consistent, the initial conditions of numerical results are assumed as $g_0 = \pi$ and $h_0 = 0$ corresponding to the resonant centre at $\sigma_{1,c} = \pi$, and they are assumed as $g_0 = 0$ and $h_0 = 0$ corresponding to the resonant centre at $\sigma_{1,c} = 0$. To produce numerical results, the equations of motion represented by Eq. (3) are numerically integrated over 500 units of dimensionless time. The orbit is recorded as a librating trajectory if the maximum variation of critical argument $\sigma = h + \text{sign}(H)g$ is smaller than 2π during the considered integration period¹⁴. The numerical distributions of apsidal reso-

nance are shown in the right panels of Figs. 8 and 9. As expected, good agreement can be found between analytical and numerical results, indicating that the resonant Hamiltonian formulated in the previous section is valid and applicable to explore dynamics of apsidal resonance under the octupole-level approximation.

5.3. Application to orbit flips

According to the results given in Fig. 7, it is known that the resonant trajectories with resonant centres at $i = 90^\circ$ can flip from prograde to retrograde and back again. In Fig. 10, analytical results of libration zones causing orbit flips are compared with the numerical distribution of flipping orbits under the octupole-level Hamiltonian model. In total, there are four libration zones causing orbit flips (zones 3, 4, 7 and 8). Inside zones 3, 4 and 8, the resonant centres are at $\sigma_{1,c} = \pi$ and, inside zone 7, the resonant centres are at $\sigma_{1,c} = 0$. Analytical results for the libration zones causing orbit flips are presented in the left panel of Fig. 10.

To be consistent with analytical results, the initial conditions of numerical results are assumed as $g_0 = 0$ and $h_0 = 0$ for the case of $\sigma_{1,c} = 0$ and they are assumed as $g_0 = 0$ and $h_0 = \pi$ for the case of $\sigma_{1,c} = \pi$. Similarly, the equations of motion are numerically integrated over 500 units of dimensionless time. The numerically propagated trajectories are recorded as flipping orbits if orbit inclinations can switch between prograde and retrograde. The numerical distribution of flipping orbits¹⁵ is shown in the right panel of Fig. 10.

¹⁴ This means that the critical argument is librating during the integration period.

¹⁵ Similar numerical results of flipping regions can be found in Lei (2022) under the dynamical model specified by $\epsilon = 0.1$. In particular, the flipping region located in the low-eccentricity space corresponds to

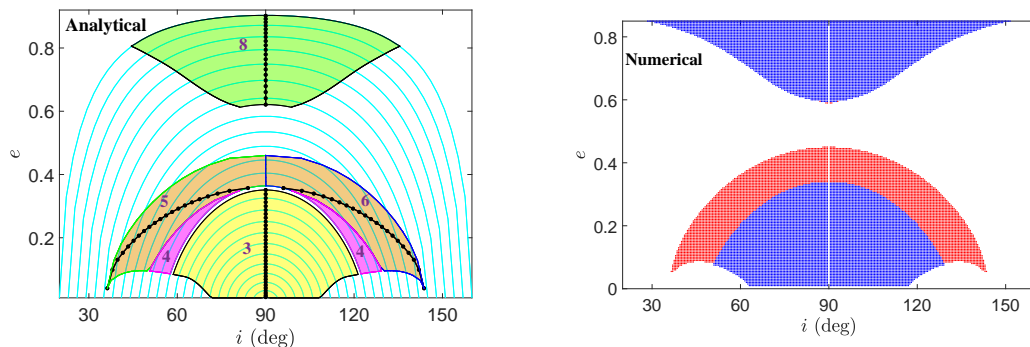


Fig. 8. Analytical results about the resonant regions for those apsidal resonances centred at $\sigma_{1,c} = \pi$ (left panel) and the associated numerical results for the distribution of apsidal resonance (right panel). For the numerical results, the initial condition is $g_0 = 0$ and $h_0 = \pi$ (corresponding to $\sigma_{1,c} = \pi$ at the initial instant). In the left panel, level curves of the motion integral Σ_2 are presented as background. In the right panel, blue dots stand for resonant trajectories inside islands centred at $i = 90^\circ$ and red dots for resonant trajectories inside asymmetric islands of libration. It should be mentioned that the difference arising in the top space is due to the fact that the analytical results are restrained by level curves of the motion integral Σ_2 .

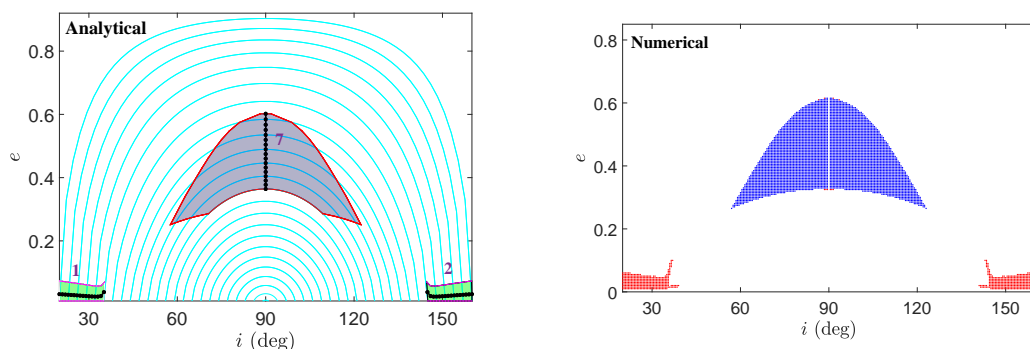


Fig. 9. Analytical results about the resonant regions for those apsidal resonances centred at $\sigma_{1,c} = 0$ (left panel) and the associated numerical results for the distribution of apsidal resonance (right panel). For the numerical results, the initial condition is $g_0 = 0$ and $h_0 = 0$ (corresponding to $\sigma_{1,c} = 0$ at the initial instant). In the left panel, level curves of the motion integral Σ_2 are presented as background. In the right panel, blue dots stand for resonant trajectories inside islands centred at $i = 90^\circ$ and red dots for resonant trajectories occurring in low-eccentricity, low-inclination spaces.

From the right panel of Fig. 10, it is observed that there are three distinct flipping regions in the (i, e) space: one located in the low-eccentricity region, one located in the intermediate-eccentricity space and the third one located in the high-eccentricity space. The low-eccentricity region of orbit flips corresponds to libration zones 3 and 4. Inside such a low-eccentricity flipping region, the critical argument $\sigma = h + \text{sign}(H)g$ is librating around π . The intermediate-eccentricity region of flipping orbits corresponds to libration zone 7, where the critical argument $\sigma = h + \text{sign}(H)g$ is librating around 0. At last, the high-eccentricity region of flipping orbits corresponds to libration zone 8, where the critical argument $\sigma = h + \text{sign}(H)g$ is librating around π .

The comparison made in Fig. 10 shows an excellent agreement between analytical and numerical results. The results imply that the dynamics of orbit flips can be well understood with the help of dynamical structures of apsidal resonance.

the LeHi case and the one located in the high-eccentricity space corresponds to the HeLi case shown in Li et al. (2014b).

6. Conclusions

In this paper, the dynamics of apsidal resonance are studied by means of perturbation treatments under the octupole-level approximation in restricted hierarchical planetary systems.

The Hamiltonian function is composed of the quadrupole-order term \mathcal{H}_2 and the octupole-order term \mathcal{H}_3 . From the viewpoint of perturbative treatments, the quadrupole-order Hamiltonian is considered as the kernel function, and the octupole-order Hamiltonian plays the role of perturbation to the quadrupole-order dynamics. By introducing the action-angle variables (a kind of canonical transformation), the quadrupole-order Hamiltonian can be converted to be independent on angular coordinates, leading to the fact that the action variables become conserved quantities under the quadrupole-order Hamiltonian flow. The transformed quadrupole-order Hamiltonian gives rise to the fundamental frequencies (or proper frequencies), which can be used to identify the nominal location of secular resonances. It is found that the secular resonances with critical argument of $\sigma = h^* + \text{sign}(H^*)g^*$ happen in the considered parameter space. We have demonstrated that, in the test-particle limit, the argument $\sigma = h^* + \text{sign}(H^*)g^*$ can be equivalently expressed as $\sigma = \varpi^* - \varpi_p$, which corresponds to apsidal resonances.

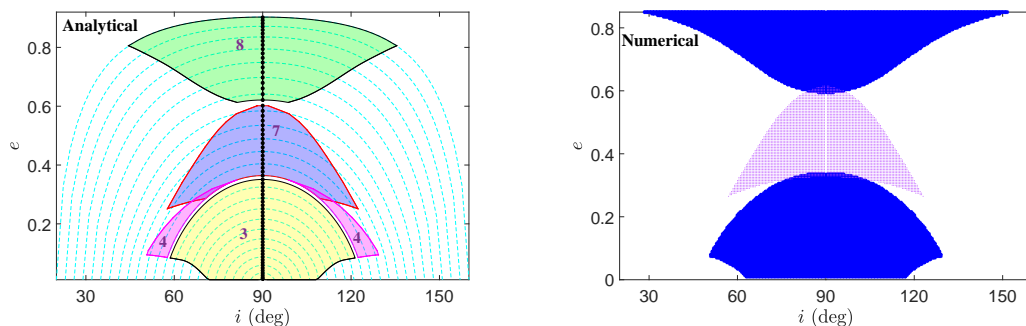


Fig. 10. Analytical results of libration zones for those apsidal resonances causing orbit flips (*left panel*) and the numerical results of flipping regions (*right panel*). In the left panel, there are four libration zones causing orbit flips (zones 3, 4, 7 and 8). It is observed that those apsidal resonances with centres at $i = 90^\circ$ cause orbit flips. In the right panel, there are three distinct regions of orbit flips, located in the low-eccentricity, intermediate-eccentricity and high-eccentricity spaces.

To study the dynamics of apsidal resonance, a canonical transformation is introduced. After transformation, it becomes a typical separable Hamiltonian model, so that we can apply first-order perturbation theory to formulate the resonant Hamiltonian model by averaging the Hamiltonian over rotating ZLK cycles. Application of first-order perturbation theory gives rise to a new constant of motion and the resulting resonant Hamiltonian model is of one degree of freedom. Phase portraits (level curves of resonant Hamiltonian with given motion integral) can be used to analyse the global dynamical structures of apsidal resonance. In particular, the location of resonance centre, saddle points, dynamical separatrix between circulating and librating regions as well as islands of libration can be determined from the resonant model.

Our main results are reported in Fig. 7. It is concluded that (a) dynamical structures are symmetric with respect to $i = 90^\circ$, (b) there are five branches of libration centres, and (c) there are eight libration zones. The comparisons between analytical and numerical results for libration zones of apsidal resonance shows good agreements between them.

It is found that islands of libration centred at $i = 90^\circ$ can cause orbit flips. Thus, those libration zones with resonant centres at $i = 90^\circ$ correspond to flipping regions in the phase space. To validate this point, the analytical results of libration zones are compared with numerical distributions of flipping orbits. A perfect correspondence can be found between the analytical and numerical results.

Through this study, we can conclude that, from the viewpoint of dynamics, the eccentric ZLK effect is equivalent to the effect of apsidal resonance at the octupole-level approximation in restricted hierarchical planetary systems. The dynamical response of the eccentric ZLK effect (or the effect of apsidal resonance) is to significantly excite eccentricities and/or inclinations (even flipping) of test particles in the very long-term evolution.

Acknowledgements

This work is supported by the National Natural Science Foundation of China (Nos 12073011, 12073019).

References

- Atognini, J. M. 2015, *MNRAS*, 452, 3610
 Ford, E. B., Kozinsky, B., & Rasio, F. A. 2000, *ApJ*, 535, 385
 Funk, B., Libert, A.-S., Süli, Á., & Pilat-Lohinger, E. 2011, *A&A*, 526, A98

- Henrard, J. 1990, *CeMDA*, 49, 43
 Henrard, J. & Lemaître, A. 1986, *Celest. Mech.*, 39, 213
 Ito, T. & Ohtsuka, K. 2019, *Monogr. Environ. Earth Planets*, 7, 1
 Katz, B., Dong, S., & Malhotra, R. 2011, *Phys. Rev. Lett.*, 107, 181101
 Kozai, Y. 1962, *AJ*, 67, 591
 Laskar, J. & Boué, G. 2010, *A&A*, 522, A60
 Lei, H. 2019, *MNRAS*, 490, 4756
 Lei, H. 2021a, *MNRAS*, 506, 1879
 Lei, H. 2021b, *CeMDA*, 133, 1
 Lei, H. 2022, *AJ*, 163, 214
 Lei, H., Circi, C., & Ortore, E. 2018, *MNRAS*, 481, 4602
 Lei, H. & Li, J. 2021, *MNRAS*, 504, 1084
 Li, G., Naoz, S., Holman, M., & Loeb, A. 2014a, *ApJ*, 791, 86
 Li, G., Naoz, S., Kocsis, B., & Loeb, A. 2014b, *ApJ*, 785, 116
 Libert, A.-S. & Delsate, N. 2012, *MNRAS*, 422, 2725
 Libert, A.-S. & Tsiganis, K. 2009, *A&A*, 493, 677
 Lidov, M. 1962, *P&SS*, 9, 719
 Lithwick, Y. & Naoz, S. 2011, *ApJ*, 742, 94
 Luo, L., Katz, B., & Dong, S. 2016, *MNRAS*, 458, 3060
 Morbidelli, A. 2002, *Modern celestial mechanics: aspects of solar system dynamics* (Taylor & Francis, London and New York)
 Naoz, S. 2016, *ARA&A*, 54, 441
 Naoz, S., Farr, W. M., Lithwick, Y., Rasio, F. A., & Teysandier, J. 2011, *Nature*, 473, 187
 Naoz, S., Farr, W. M., Lithwick, Y., Rasio, F. A., & Teysandier, J. 2013, *MNRAS*, 431, 2155
 Shevchenko, I. I. 2016, *The Lidov-Kozai effect-applications in exoplanet research and dynamical astronomy*, Vol. 441 (Springer)
 Sidorenko, V. V. 2018, *CeMDA*, 130, 4